Communication

Model Order Reduction in Hybrid Methods Involving Generalized Impedance Matrix

Grzegorz Fotyga, Damian Szypulski, Rafal Lech, Piotr Kowalczyk

***Abstract*—A novel strategy for the efficient analysis of frequency-domain scattering electromagnetic problems in open and closed domains is presented. A fully automatic model-order reduction technique, called the enhanced reduced-basis method, is applied to increase the efficiency of the hybrid approach, which combines the finite-element and mode-matching methods. Numerical tests show that the proposed algorithm yields reliable and highly accurate results whereas the computational time is reduced by up to one order of the magnitude.**

***Index Terms*—model-order reduction, *a posteriori* error estimator, finite element method.**

I. Introduction

In general, there are three different classes of electromagnetic structure analysis methods. For structures with simple geometries, it is efficient to utilize analytical approaches (e.g. the mode-matching (MM) method), which are very efficient and accurate [1]–[4]. However, their flexibility is limited, and usually they are dedicated to specific structural shapes. For complex structures, a variety of discrete methods is available [5], [6] (e.g. finite difference (FD) or finite element method (FEM)), but their numerical cost is much higher, which results in low efficiency in the design and optimization process. In some cases (e.g. multi-scale structures), the requirement for computational resources is too high, which makes these methods useless from a practical point of view.

The solution to these problems is the hybridization of both method classes, which combines their advantages. Such an approach has been known for over two decades [7]–[12] and is successfully applied even in commercial software [13]. The idea of the hybrid methods is the utilization of discrete methods only for small fragments of the structure (discrete regions), whereas the rest of the computational domain is analyzed analytically (analytical regions) [8], [11], [12], [14]. One of the most common hybrid approaches is based on a Generalized Impedance Matrix (GIM) [8], [15], which relates electric and magnetic fields defined on the boundary of a discrete region. This approach allows the discrete regions to be replaced by objects described by the GIMs in further (analytical) analysis.

Manuscript received MM DD, 20YY; revised MM DD, 20YY. This work was supported by the TEAM-TECH project entitled EDISOn—Electromagnetic Design of flexIble SensOrs—operated within the Foundation for Polish Science TEAM-TECH Programme, co-financed by the European Regional Development Fund, Smart Growth Operational Programme 2014–2020.

The authors are with the Department of Microwave and Antenna Engineering, Faculty of Electronics, Telecommunications and Informatics, Gdansk University of Technology, Gdansk, 80-233 Poland (e-mail: grzfotyg@pg.gda.pl, damian.szypulski@pg.edu.pl, rlech@eti.pg.edu.pl, pio.kow@gmail.com, m.mrozowski@ieee.org)

However, if the analysis requires the structures to be characterized in a wide frequency band, the computation of the GIM has to be performed for each of the frequency points independently. For complex structures, the number of frequency points has to be significantly large, and even the utilization of the hybrid method can be time-consuming. In order to improve the efficiency of the frequency-domain analysis, the model-order reduction (MOR) techniques can be applied [16]–[21]. They have been proved to be reliable and able to significantly speed up computations.

The main contribution of this paper is to provide the theoretical background of the model-order reduction approach, called the Enhanced Reduced Basis Method (EnRBM) [21], applied to the GIM-based hybrid technique, and compare it to the popular Fast Frequency Sweep (FFS) algorithms. Also, the formula for an efficient and reliable error estimator is derived. It allows the reduction process to be fully automated in terms of the accuracy of the generated reduced-order model. In order to verify the reliability of the proposed approach, two different problems are examined, namely scattering in an open space, and in a waveguide junction. Finally, the efficiency of the two different libraries used to solve the FEM system of equations are compared: Unsymmetric MultiFrontal PACKage [22] and Intel Math Kernel Library Parallel Direct Sparse Solver Interface [23].

II. Hybrid Method with GIM

The main idea of the hybrid method involving the GIM is based on division of the computational domain into regions where analytical methods can be utilized, and parts where discrete methods are more suitable. The discrete parts of the domain are surrounded by artificial boundaries (preferably with simple geometries) on the surfaces of which the relations between electric and magnetic fields are calculated. This approach allows the discrete regions to be replaced by objects described by the GIMs in further analysis.

A. Definition of GIM

Since the tangential components of electric and magnetic fields at the artificial boundaries can be expressed by chosen series of appropriate basis functions with field coefficients $\mathbf{V}$ and $\mathbf{I}$, in practice the GIM $\mathbf{Z}$ represents the relation between these coefficients:

$$\mathbf{V} = \mathbf{Z}\mathbf{I} \tag{1}$$

Due to the simplicity of the description of the issue, we will focus on the GIM in two dimensional cases (involving

This article has been accepted for publication in a future issue of this journal, but has not been fully edited. Content may change prior to final publication. Citation information: DOI 10.1109/TAP.2020.2970027, IEEE Transactions on Antennas and Propagation

open and closed structures), however the presented idea is also applicable in the analysis of three dimensional problems. The investigated structures are presented in Fig. 1. The first is a single, infinitely long cylindrical post of arbitrary cross-section surrounded by an artificial circular cylinder, and obliquely illuminated by a plane wave. The second is a waveguide junction field with posts of arbitrary cross-sections homogeneous along their heights. In both cases, the post axis is located along the z-axis in the coordinate system. Therefore, regardless of type of excitation, the tangential electric and magnetic fields on the artificial boundary surrounding the discrete region can be expanded with the following series:

$$\vec{E}_z = \sum_m V_{TM,m}\vec{e}_{z,m}, \quad \vec{E}_t = \sum_m V_{TE,m}\vec{e}_{t,m}, \quad (2)$$

$$\vec{H}_z = \sum_m I_{TE,m}\vec{h}_{z,m}, \quad \vec{H}_t = \sum_m I_{TM,m}\vec{h}_{t,m}, \quad (3)$$

where $V_{(\cdot)m}$ and $I_{(\cdot)m}$ are the field coefficients of the assumed field expansion functions $\vec{e}_{(\cdot)m}$ and $\vec{h}_{(\cdot)m}$ (the forms of $\vec{e}_{(\cdot)m}$ and $\vec{h}_{(\cdot)m}$ and the range of mode numbers m depend on the investigated problem, as discussed in the next paragraphs). The subscript t denotes another tangential component (φ in the cylindrical coordinate system, and y in the rectangular coordinate system - see Fig. 1).

In the case of scattering problems, assuming the boundary is being represented by a cylindrical surface, it is convenient to take the following expansion functions:

$$\vec{e}_{z,m}(\varphi,z) = e^{-jk_z z}e^{jm\varphi}\vec{i}_z, \quad \vec{e}_{t,m}(\varphi,z) = -e^{-jk_z z}e^{jm\varphi}\vec{i}_\varphi,$$
$$\vec{h}_{z,m}(\varphi,z) = e^{-jk_z z}e^{jm\varphi}\vec{i}_z, \quad \vec{h}_{t,m}(\varphi,z) = e^{-jk_z z}e^{jm\varphi}\vec{i}_\varphi,$$

for $m \in \{-M,...,M\}$, where $\vec{i}_{(\cdot)}$ are the unit vectors of the considered coordinate system, $k_z = k_0\cos\theta_0$, k_0 is the wavenumber of the free space, θ_0 is the angle of plane wave incidence with respect to the object axis, and the number of functions used in expansion is equal to $2M+1$. Due to the arbitrary value of the incident angle θ_0, the problem must be defined using a scalar-vector formulation. Therefore, both wave polarizations TE and TM with respect to the z-axis need to be taken into consideration and the GIM can be expressed in the following form:

$$\begin{bmatrix}\mathbf{V}_{TM}\\ \mathbf{V}_{TE}\end{bmatrix} = \begin{bmatrix}\mathbf{Z}_{TM,TM} & \mathbf{Z}_{TM,TE}\\ \mathbf{Z}_{TE,TM} & \mathbf{Z}_{TE,TE}\end{bmatrix}\begin{bmatrix}\mathbf{I}_{TM}\\ \mathbf{I}_{TE}\end{bmatrix} \quad (4)$$

where $\mathbf{V}_{(\cdot)}$ and $\mathbf{I}_{(\cdot)}$ are column vectors of the field coefficients.

In the case of the waveguide junction, the boundary is represented by a rectangular surface. Assuming that the object height extends over the entire junction, it is sufficient to consider only TM_{m0} modes, so the problem can be defined using a scalar formulation. Therefore, only one polarization (TM) of the electric and magnetic fields on the artificial boundaries (in both waveguide ports) can be used in the expansion series (2) and (3). In this case, it is convenient to use the following expansion functions:

$$\vec{e}_{z,m}(y) = \begin{cases}\sin(\frac{m\pi y}{a})\vec{i}_z, & m = 1,..,M\\ \sin(\frac{(m-M)\pi y}{a})\vec{i}_z, & m = M+1,..,2M\end{cases}$$

$$\vec{h}_{t,m}(y) = \begin{cases}\sin(\frac{m\pi y}{a})\vec{i}_y, & m = 1,..,M\\ -\sin(\frac{(m-M)\pi y}{a})\vec{i}_y, & m = M+1,..,2M\end{cases}$$

where a is a width of the waveguide. The numbering of basis functions in the range $m = 1,...,M$ is related to port 1 and in the range $m = M+1,...,2M$ to port 2. Due to the above assumptions, the GIM in this case can be expressed in the following simpler form:

$$\mathbf{V}_{TM} = \mathbf{Z}_{TM,TM}\mathbf{I}_{TM} \quad (5)$$

B. Calculation of GIM with FEM

The electric field in the discrete region can be expressed utilizing standard hierarchical basis functions [24] $\alpha_{(\cdot)}^{[n]}$ and $\vec{W}_{(\cdot)}^{[n]}$ of the second order:

$$E_z = \sum_{n=1}^{N}\sum_{i=1}^{6}\Psi_{(i)}^{[n]}\alpha_{(i)}^{[n]}, \quad \vec{E}_t = \sum_{n=1}^{N}\sum_{i=1}^{8}\Phi_{(i)}^{[n]}\vec{W}_{(i)}^{[n]} \quad (6)$$

where $n = 1,\ldots,N$ is the element number, i represents the local node/edge, and $\Psi_{(i)}^{[n]}$ and $\Phi_{(i)}^{[n]}$ are unknown coefficients for the scalar and vector components, respectively.

Using the FEM, the problem boils down to the system of equations (the details can be found in [14]):

$$\begin{bmatrix}\Psi(k_0)\\ \Phi(k_0)\end{bmatrix} = \mathbf{G}(k_0)^{-1}j\omega\mu_0\mathbf{B}\begin{bmatrix}\mathbf{I}_{TM}\\ \mathbf{I}_{TE}\end{bmatrix}. \quad (7)$$

Global matrices $\mathbf{G} \in \mathbb{C}^{N\times N}$ and $\mathbf{B} \in \mathbb{C}^{N\times(4M+2)}$ can be obtained from the aggregation of local matrices [14]:

$$\mathbf{G}(k_0) = \begin{bmatrix}\mathbf{G}_{TM,TM} & \mathbf{G}_{TM,TE}\\ \mathbf{G}_{TE,TM} & \mathbf{G}_{TE,TE}\end{bmatrix}, \mathbf{B} = \begin{bmatrix}\mathbf{B}_{TM} & \mathbf{0}\\ \mathbf{0} & \mathbf{B}_{TE}\end{bmatrix} \quad (8)$$

where the local matrices are frequency-dependent:

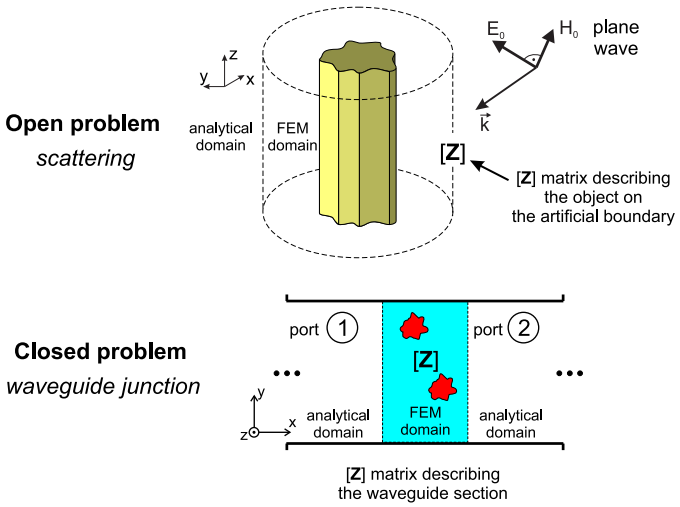

Fig. 1. Examined examples: plane wave scattering and waveguide junction

This article has been accepted for publication in a future issue of this journal, but has not been fully edited. Content may change prior to final publication. Citation information: DOI 10.1109/TAP.2020.2970027, IEEE Transactions on Antennas and Propagation

$$\begin{aligned}
\left[\mathbf{G}^{[n]}_{TM,TM}\right]_{p,i} &= -k_0^2 \iint_{S^{[n]}} \alpha^{[n]}_{(p)} \varepsilon_{rz} \alpha^{[n]}_{(i)} ds \\
&\quad - \iint_{S^{[n]}} \vec{\nabla}_t \alpha^{[n]}_{(p)} \cdot \left[\vec{i}_z \times \bar{\mu}^{-1}_{rt} \left(\vec{i}_z \times \vec{\nabla}_t \alpha^{[n]}_{(i)}\right)\right] ds, \\
\left[\mathbf{G}^{[n]}_{TM,TE}\right]_{p,i} &= \\
&\quad -jk_z \iint_{S^{[n]}} \vec{\nabla}_t \alpha^{[n]}_{(p)} \cdot \left[\vec{i}_z \times \bar{\mu}^{-1}_{rt} \left(\vec{i}_z \times \vec{W}^{[n]}_{(i)}\right)\right] ds, \\
\left[\mathbf{G}^{[n]}_{TE,TM}\right]_{p,i} &= \\
&\quad jk_z \iint_{S^{[n]}} \vec{W}^{[n]}_{(p)} \cdot \left[\vec{i}_z \times \bar{\mu}^{-1}_{rt} \left(\vec{i}_z \times \nabla_t \alpha^{[n]}_{(i)}\right)\right] ds, \\
\left[\mathbf{G}^{[n]}_{TE,TE}\right]_{p,i} &= -k_0^2 \iint_{S^{[n]}} \vec{W}^{[n]}_{(p)} \cdot \bar{\varepsilon}_{rt} \vec{W}^{[n]}_{(i)} \, ds \\
&\quad \iint_{S^{[n]}} \left(\vec{\nabla}_t \times \vec{W}^{[n]}_{(p)}\right) \cdot \left(\mu^{-1}_{rz} \vec{\nabla}_t \times \vec{W}^{[n]}_{(i)}\right) ds \\
&\quad -k_z^2 \iint_{S^{[n]}} \vec{W}^{[n]}_{(p)} \cdot \left[\vec{i}_z \times \bar{\mu}^{-1}_{rt} \left(\vec{i}_z \times \vec{W}^{[n]}_{(i)}\right)\right] ds, \\
\left[\mathbf{B}^{[n]}_{TM}\right]_{p,m} &= \int_{L \cap L^{[n]}} \alpha^{[n]}_{(p)} \vec{i}_z \cdot (\vec{n}_m \times \vec{h}_{tm}) dl, \\
\left[\mathbf{B}^{[n]}_{TE}\right]_{p,m} &= \int_{L \cap L^{[n]}} \vec{W}^{[n]}_{(p)} \cdot (\vec{n}_m \times \vec{h}_{zm}) dl,
\end{aligned} \tag{9}$$

where $\bar{\varepsilon}_r$ and $\bar{\mu}_r$ are the tensor relative permittivity and permeability, respectively, defined in [14]. In the scattering case, the normal unit vector $\vec{n}_m = \vec{i}_\rho$, whereas for the waveguide problem, $\vec{n}_m = \vec{i}_x$ for $m = 1, ..., M$ and $\vec{n}_m = -\vec{i}_x$ for $m = M+1, ..., 2M$.

For the sake of clarity, the local $\mathbf{G}$ matrices can be presented in the short, matrix form, based on (9):

$$\begin{aligned}
\mathbf{G}_{TM,TM}(k_0) &= -\mathbf{C}_s - k_0^2 \mathbf{T}_s, \\
\mathbf{G}_{TM,TE}(k_0) &= -jk_0 \mathbf{S}_{sv}, \\
\mathbf{G}_{TE,TM}(k_0) &= jk_0 \mathbf{S}^H_{sv}, \\
\mathbf{G}_{TE,TE}(k_0) &= \mathbf{C}_v - k_0^2 \mathbf{T}_v - k_0^2 \mathbf{\Gamma}_v
\end{aligned} \tag{10}$$

where indices s and v correspond to the scalar and vector parts, respectively. Grouping together the constant, linear and quadratic terms from (10), the affine formula is obtained:

$$\mathbf{G}(k_0) = \mathbf{G}_0 + k_0 \mathbf{G}_1 + k_0^2 \mathbf{G}_2 \tag{11}$$

where:

$$\begin{aligned}
\mathbf{G}_0 &= \begin{bmatrix} -\mathbf{C}_s & 0 \\ 0 & \mathbf{C}_v \end{bmatrix}, \quad \mathbf{G}_1 = \begin{bmatrix} 0 & -j\mathbf{S}_{sv} \\ j\mathbf{S}^H_{sv} & 0 \end{bmatrix}, \\
\mathbf{G}_2 &= \begin{bmatrix} -\mathbf{T}_s & 0 \\ 0 & -\mathbf{T}_v - \mathbf{\Gamma}_v \end{bmatrix}.
\end{aligned} \tag{12}$$

Finally, the impedance matrix, which can be treated as an input to the output frequency-dependent transfer function, is:

$$\mathbf{Z}(k_0) = \Delta^{-1} \mathbf{B}^H \mathbf{G}(k_0)^{-1} j\omega\mu_0 \mathbf{B}. \tag{13}$$

In the case of scattering, $\Delta = 2\pi R$ is a scalar value, and R is the radius of the artificial cylinder. For the waveguide problem, Δ is a diagonal matrix of the form:

$$\Delta_{m,m} = -\frac{a}{2} \begin{cases} \sqrt{\left(\frac{m\pi}{a}\right)^2 - k_0^2}, & m = 1, .., M \\ \sqrt{\left(\frac{(m-M)\pi}{a}\right)^2 - k_0^2}, & m = M+1, .., 2M \end{cases} \tag{14}$$

C. Matching GIM with external field

Calculation of the GIM is performed in isolation from external excitation. Therefore, this matrix, in further analysis, describes the region composed a complex object, or group of objects, and can be matched with any known external incident fields (e.g. a plane wave illuminating the object or a waveguide field exciting the junction). For instance, calculating the GIM on a circular cylinder surrounding a post with complex geometry allows us to treat this object as a simple cylinder and its further analysis can be performed with the use of analytical methods. The procedure consists of writing the impedance relation between known incident field and unknown scattered (reflected and/or transmitted) field on the artificial boundary where the GIM is defined, and then using the GIM to calculate field coefficients of the scattered field.

III. Model order reduction

In order to obtain the scattering characteristics of the analyzed structure using the method described in Section II, the $\mathbf{Z}(k_0)$ matrix has to be computed at each of the selected frequency points in the bandwidth $[k_{0_{min}}, k_{0_{max}}]$. However, if the computational domain is complex, the number of FEM variables is large and the computations become time-consuming. To increase the efficiency of the computations, the model-order reduction methods can be of help, which leads to the reduced-order system of (7) defined as:

$$\begin{bmatrix} \widetilde{\Psi}(k_0) \\ \widetilde{\Phi}(k_0) \end{bmatrix} = (k_0^2 \widetilde{\mathbf{G}}_2 + k_0 \widetilde{\mathbf{G}}_1 + \widetilde{\mathbf{G}}_0)^{-1} j\omega\mu_0 \widetilde{\mathbf{B}} \begin{bmatrix} \mathbf{I}_{TM} \\ \mathbf{I}_{TE} \end{bmatrix} \tag{15}$$

where the reduced blocks $\widetilde{\mathbf{G}}_0, \widetilde{\mathbf{G}}_1, \widetilde{\mathbf{G}}_2 \in \mathbb{C}^{\widetilde{N} \times \widetilde{N}}$ and $\widetilde{\mathbf{B}} \in \mathbb{C}^{\widetilde{N} \times (4M+2)}$ (with $\widetilde{N} \ll N$) are obtained using Galerkin projection of the original FEM system matrices onto a subspace spanned by the vectors of the orthogonal basis $\mathbf{Q}$:

$$\widetilde{\mathbf{G}}_0 = \mathbf{Q}^H \mathbf{G}_0 \mathbf{Q}, \quad \widetilde{\mathbf{G}}_1 = \mathbf{Q}^H \mathbf{G}_1 \mathbf{Q}, \quad \widetilde{\mathbf{G}}_2 = \mathbf{Q}^H \mathbf{G}_2 \mathbf{Q} \tag{16}$$

$$\widetilde{\mathbf{B}} = \mathbf{Q}^H \mathbf{B}. \tag{17}$$

Similarly, the reduced transfer function, which aims to approximate the original transfer function with sufficient accuracy, is defined as follows:

$$\widetilde{\mathbf{Z}}(k_0) = \Delta^{-1} \widetilde{\mathbf{B}}^H (k_0^2 \widetilde{\mathbf{G}}_2 + k_0 \widetilde{\mathbf{G}}_1 + \widetilde{\mathbf{G}}_0)^{-1} j\omega\mu_0 \widetilde{\mathbf{B}}. \tag{18}$$

In the reduced-basis method (RBM) case [18], [19] the projection basis $\mathbf{Q}$ is composed of the solutions of (7) (called snapshots), computed at several properly selected points [18]:

$$colsp\{\mathbf{Q}\} = span\left\{ \begin{bmatrix} \Psi(k_0^1) \\ \Phi(k_0^1) \end{bmatrix}, \ldots, \begin{bmatrix} \Psi(k_0^J) \\ \Phi(k_0^J) \end{bmatrix} \right\} \tag{19}$$

This article has been accepted for publication in a future issue of this journal, but has not been fully edited. Content may change prior to final publication. Citation information: DOI 10.1109/TAP.2020.2970027, IEEE Transactions on Antennas and Propagation

where J is the number of expansion points, at which the snapshots are generated. The number and the placement of the expansion points follows the strategy described in [21]. More precisely, the algorithm starts with the three snapshots placed in the middle and at the sides of the band. The placement of subsequent expansion points is determined following the greedy strategy, i.e. the next snapshot is computed at the frequency for which the error of the reduced-order model is maximum, i.e. for the frequency at which the approximation of the original model by the reduced one is the worst.

In order to efficiently assess the error introduced by the reduced model, residual error-based error estimation is utilized. The residual error is defined as follows:

$$\mathbf{R}(f) = j\omega\mu_0\mathbf{B} - \mathbf{G}\mathbf{Q}\begin{bmatrix}\widetilde{\Psi}\\ \widetilde{\Phi}\end{bmatrix} \tag{20}$$

where the unit amplitudes of the input excitation are assumed, and $[\widetilde{\Psi}^T, \widetilde{\Phi}^T]^T$ is computed by means of (15). We are interested in obtaining the $\mathbf{Z}$ parameters of subregion, which are associated with the artificial boundary between the two domains (see Fig. 1 for details). Therefore, the most appropriate error estimator definition is the goal-oriented one, which takes into account the interaction between the residual error and the right-hand side matrix $\mathbf{B}$:

$$\begin{aligned}\mathbf{e}_{est}(k_0) &= \|j\omega\mu_0\mathbf{B^H}\mathbf{R}\|_2/\|(j\omega\mu_0)^2\mathbf{B^H}\mathbf{B}\|_2\\ &= \|\big[(j\omega\mu_0)^2\mathbf{B^H}\mathbf{B} - j\omega\mu_0(\mathbf{B^H}\mathbf{G}_0\mathbf{Q} + k_0\mathbf{B^H}\mathbf{G}_1\mathbf{Q}\\ &+ k_0^2\mathbf{B^H}\mathbf{G}_2\mathbf{Q})[\widetilde{\Psi}^T \quad \widetilde{\Phi}^T]^T\big]\|_2/\|(j\omega\mu_0)^2\mathbf{B^H}\mathbf{B}\|_2\end{aligned} \tag{21}$$

Note that the matrices $\mathbf{Q}, \mathbf{B}, \mathbf{G}_0, \mathbf{G}_1$ and $\mathbf{G}_2$ are frequency independent, thus the components $\mathbf{B}^H\mathbf{G}_0\mathbf{Q}$, $\mathbf{B}^H\mathbf{G}_1\mathbf{Q}$, $\mathbf{B}^H\mathbf{G}_2\mathbf{Q}$ and $\mathbf{B}^H\mathbf{B}$ are computed only once, in the so-called *offline* stage. Since the error estimator operates on small blocks of matrices, it is computed extremely quickly. It is used not only to determine the subsequent expansion points, but also to stop the RBM approach once the estimated error drops below the assumed tolerance.

IV. Results

In this section, the two numerical tests which illustrate the proposed method are considered. All the computations were performed in Matlab on an Intel i5-7400 workstation with 32GB RAM. The systems of equations obtained from FEM were solved both by means of the MKL PARDISO sparse solver [23] and the UMFPACK [22] library.

A. Scattering from cylindrical object

The first numerical test dealt with plane wave scattering from a cylindrical object with a star-shaped cross-section, as illustrated schematically in Fig. 2. The goal of the computations was to obtain the scattering characteristics of the structure in the frequency band $9 - 11$ GHz.

The first simulation was performed by means of the standard FEM formulation with the computational domain truncated by means of the perfectly matched layer (PML).

Assuming an oblique angle of plane wave incidence ($\theta_0 = 30^\circ$ and $\phi_0 = 30^\circ$), all the field components needed to be considered, thus the FEM analysis was formulated as a vector-scalar deterministic problem. The overall simulation (in 201 equidistant frequency-points) took 405.2 s and 381.1 s for UMFPACK and MKL PARDISO, respectively. It should be noted that, in this case, the dominant numerical effort is devoted for the PML computation, not for the solution of FEM system of equations. This is the reason that the difference between the MKL and UMFPACK computational times in this case is insignificant.

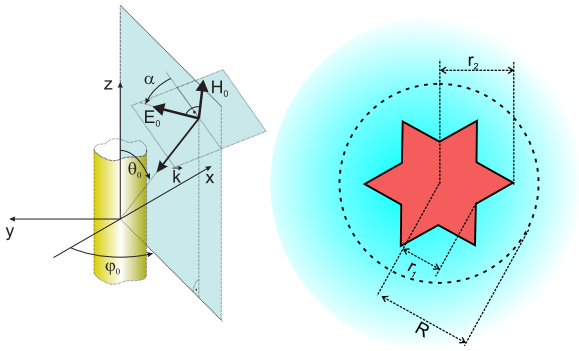

Fig. 2. Examined example of open structure: plane wave scattering, R=29.90 mm, $r_1 = 17.94$ mm, $r_2 = 22.42$ mm

Next, the scattering field was computed using the hybrid method described in Section II. To this end, the computational domain was enclosed by a cylindrical surface with $R = 29.9$ mm. Due to the FEM discretization of the inner region, a system of equations with 44079 unknowns was generated, whereas the number of right-hand side (RHS) vectors is 62 (with M = 15). As in the first case, the problem was solved in 201 frequency points, using the two libraries, UMFPACK and MKL PARDISO, which took 80.5 s and 301.1 s, respectively. The plots of the normalized scattered far-field as a function of frequency and φ is presented in Fig 3. Finally, the problem was analyzed by means of the proposed MOR method described in Section III. The first three snapshots were located in the middle and at the band ends. The placement of subsequent snapshots was computed following the greedy approach. Due to the reduction process a projection basis $\mathbf{Q}$ which consists of 372 vectors, expanded in 6 frequency points, was generated. Fig. 4 shows the plots of the real and estimated errors, where

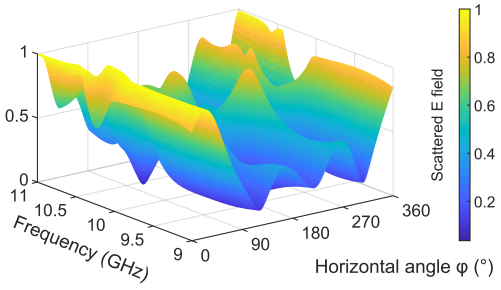

Fig. 3. The plots of the normalized scattered far-field as a function of frequency and angle φ.

This article has been accepted for publication in a future issue of this journal, but has not been fully edited. Content may change prior to final publication. Citation information: DOI 10.1109/TAP.2020.2970027, IEEE Transactions on Antennas and Propagation

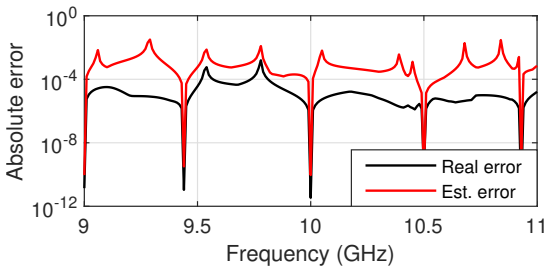

Fig. 4. Near field real error compared to residual estimated error.

TABLE I
NUMERICAL RESULTS, SCATTERING FROM STAR

	PARDISO	UMFPACK
Full FEM time [s]	381.1	405.2
Hybrid time [s]	80.5	301.1
Hybrid+MOR time [s]	18.3	24.5
MOR time [s]	15.0	21.2
Speedup (total / reduction)	**20.8 / 4.4**	**16.5 / 12.3**
Projection basis size	372	372
Maximum estimate error	1.3e-03	1.3e-03
Maximum far-field real err	2.6e-11	2.9e-10

the real one is defined as:

$$\mathbf{e}_{real}(k_0) = \|(\mathbf{Q}[\widetilde{\Psi}(k_0)^T\ \widetilde{\Phi}(k_0)^T]^T - [\Psi(k_0)^T\ \Phi(k_0)^T]^T)\|_2 / \|[\Psi(k_0)^T\ \Phi(k_0)^T]^T\|_2. \quad (22)$$

It can be seen that both errors are well-correlated in the whole band and the real error is bounded by the estimated one. Finally, the real error in the far-field zone, was computed, and the results are presented in Fig. 5. It is defined as:

$$\mathbf{e}_{farfield}(k_0) = \|(\vec{e}_{real} - \vec{e}_{MOR})\|_2 / \|(\vec{e}_{real})\|_2. \quad (23)$$

The results of simulations by means of MKL PARDISO and UMFPACK are summarized in Tab. I. The proposed MOR method took 18.2 s, which resulted in a computational speed-up equal to 4.4 and 20.8 for the standard hybrid method and PML, respectively. It can be seen that the real error in the far-field zone is much below the real error of the near field, therefore the tolerance of the reduced-order model set to $1e-2$ is sufficient. The goal of the last simulation was to study the speed-up of MOR computations with respect to the hybrid method as function of the number of frequency

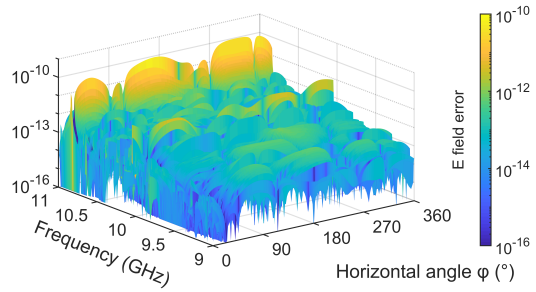

Fig. 5. Far field real error.

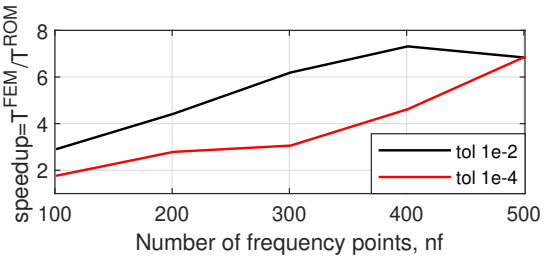

Fig. 6. Speed-up of computations in terms of the number of frequency points and the tolerance.

points, varying from 101 to 501, and the tolerance level equal to 1e-2 and 1e-4, using MKL PARDISO. The results of the simulations are presented in Fig. 6. As can be seen, the speed-up of computations increases with the number of frequency points.

B. Periodic structure in rectangular waveguide

The second numerical experiment deals with a pseudo-periodic structure composed of twenty identical sections of double dielectric rectangular posts located in a rectangular waveguide as schematically illustrated in Fig. 7. The goal of the analysis was to obtain the scattering parameters of the structure in the band $9-17$ GHz. In the first simulation, a single section of length D was analyzed using the standard FEM formulation, with $N = 42903$ (both regions 1 and 2 were analyzed with the FEM method). Next, the scattering matrix of a single section was computed, and used to obtain the scattering characteristics of the whole structure, by cascading scattering matrices of twenty section (Fig. 8). The whole simulation (in 501 frequency points) took 84.9 s and 1157.6 s with MKL PARDISO and UMFPACK, respectively. In the second simulation, we utilized the hybrid method described in Section II. To this end, we divided a single section into two subdomains (regions 1 and 2), analyzed independently using FEM (in region 2) and the analytic method (in region 1). The field at the boundary between subdomains was expanded into a series of 30 functions (corresponding to $M = 15$). Next, the FEM system of equations with $N = 19623$ was generated and as in the first case, the scattering parameters of the whole structure were computed. The analysis took 38.3 s and 401.2 s (using MKL PARDISO and UMFPACK).

Finally, the structure was simulated by means of the proposed MOR approach. As in the first case, the tolerance was set to $1e-2$. The reduced-order model was generated following the greedy strategy of snapshot selection, based on the error

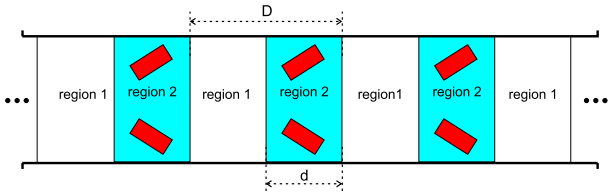

Fig. 7. Examined example of closed structure: periodic structure in rectangular waveguide

This article has been accepted for publication in a future issue of this journal, but has not been fully edited. Content may change prior to final publication. Citation information: DOI 10.1109/TAP.2020.2970027, IEEE Transactions on Antennas and Propagation

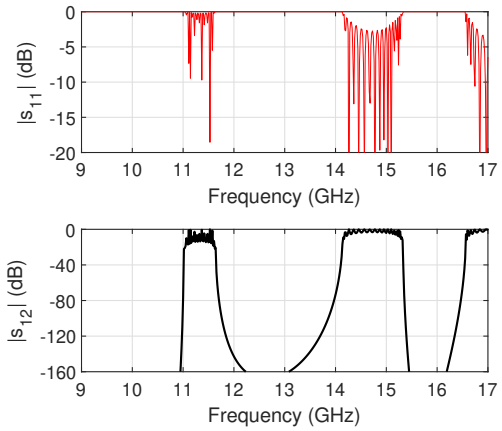

Fig. 8. Scattering parameters of periodic structure

TABLE II
NUMERICAL RESULTS, PERIODIC STRUCTURE

	PARDISO	UMFPACK
Full FEM time	84.9	1157.6
Hybrid time	38.3	401.2
Hybrid+MOR time	5.9	8.7
MOR time [s]	3.0	5.7
Speedup (total / reduction)	**14.4 / 6.5**	**133.1 / 46.1**
Projection basis size	120	120
Maximum estimate error	3.1e-06	3.1e-06

estimator. Finally, the projection basis was composed of 4 snapshots (120 vectors), which resulted in the maximum value of the estimated and the real errors at the level of $3.1e-6$ and $5.3e-8$, respectively. The error plots as a function of frequency are shown in Fig. 9. Note that the real error for a single section as well as for the whole structure are provided. The results of simulation are presented in Tab. II. As in the first numerical test, the MKL PARDISO library solved the FEM system of equations significantly faster compared to UMFPACK. The reduction speed-up of computations with respect to the hybrid method is equal to 6.5 and 46.1 for MKL PARDISO and UMFPACK, respectively, whereas the total speed-up with respect to the full FEM is 14.4 and 133.1.

C. Comparison to other FFS methods

The aim of the last numerical test was to compare the proposed MOR approach to the two popular Fast Frequency Sweep (FFS) methods. The first is a single-point moment-matching approach called SAPOR [16]. The second is the matrix interpolation method, based on Vector Fitting [25]. It generates the rational function formulas, to represent each of the impedance matrix elements. The tests showed that the first approach leads to overgrown projection bases, whereas the second requires a much higher number of FEM system matrix factorizations (compared to EnRBM) to converge at a similar level of error. For example, in the periodic structure case (Section IV-B), to perform FFS, we needed as many as 4 factorizations using EnRBM, and 20 factorizations using

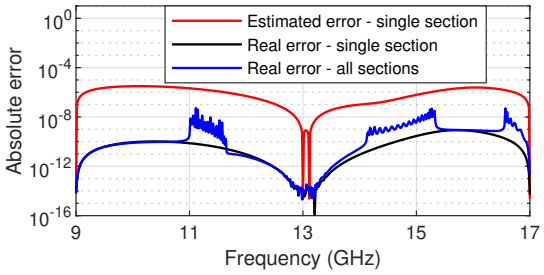

Fig. 9. Estimated and real errors of periodic structure.

matrix interpolation. In effect, for the analyzed cases, both methods are inefficient, as compared to EnRBM.

V. CONCLUSIONS

In this letter, a systematic model-order reduction process has been presented for enhancing the efficiency of frequency-domain analyses, performed by means of the hybrid method, which combines the finite-element and mode-matching methods. The numerical tests confirm that the proposed approach results in a significant reduction of the number of variables, as well as the simulation time.

REFERENCES

[1] J. Kong, L. Tsang, and K. Ding, "Scattering of Electromagnetic Waves, Theories and Applications, vol. 1," 2000.
[2] A. Elsherbeni, M. Hamid, and G. Tian, "Iterative scattering of a Gaussian beam by an array of circular conducting and dielectric cylinders," *J. Electromagn. Waves Appl.*, vol. 7, no. 10, pp. 1323–1342, 1993.
[3] R. Gesche and N. Lochel, "Scattering by a lossy dielectric cylinder in a rectangular waveguide," *IEEE Trans. Microw. Theory Techn.*, vol. 36, no. 1, pp. 137–144, Jan. 1988.
[4] H. Nakano, "Analysis methods for electromagnetic wave problems," *Yamashita Ed., Norwood, MA: Artech House*, vol. 2, pp. 20–10, 1996.
[5] D. B. Davidson, *Computational electromagnetics for RF and microwave engineering*. Cambridge University Press, 2010.
[6] A. Taflove and S. C. Hagness, *Computational electrodynamics: the finite-difference time-domain method*. Artech house, 2005.
[7] X.-Q. Sheng, J.-M. Jin, J. Song, C.-C. Lu, and W. C. Chew, "On the formulation of hybrid finite-element and boundary-integral methods for 3-D scattering," *IEEE Trans. Antennas Propag.*, vol. 46, no. 3, pp. 303–311, Mar. 1998.
[8] J. Rubio, J. Arroyo, and J. Zapata, "Analysis of passive microwave circuits by using a hybrid 2-D and 3-D finite-element mode-matching method," *IEEE Trans. Microw. Theory Techn.*, vol. 47, no. 9, pp. 1746–1749, Sep. 1999.
[9] D. Arena, M. Ludovico, G. Manara, and A. Monorchio, "A hybrid mode matching/FEM technique with edge elements for solving waveguides discontinuity problems," in *Antennas and Propagation Society International Symposium, 2000. IEEE*, vol. 4. IEEE, 2000, pp. 2028–2031.
[10] M. G. de Aza, J. A. Encinar, J. Zapata, and M. Lambea, "Full-wave analysis of cavity-backed and probe-fed microstrip patch arrays by a hybrid mode-matching generalized scattering matrix and finite-element method," *IEEE Trans. Antennas Propag.*, vol. 46, no. 2, pp. 234–242, Feb. 1998.
[11] A. Kusiek, R. Lech, and J. Mazur, "A new hybrid method for analysis of scattering from arbitrary configuration of cylindrical objects," *IEEE Trans. Antennas Propag.*, vol. 56, no. 6, pp. 1725–1733, Jun. 2008.
[12] A. Kusiek and J. Mazur, "Application of hybrid finite-difference mode-matching method to analysis of structures loaded with axially symmetrical posts," *Microw. Opt. Technol. Lett.*, vol. 53, no. 1, pp. 189–194, Apr. 2011.
[13] E. FEKO, "Software & systems sa,(pty) ltd, 32 techno lane," *Technopark, Stellenbosch*, vol. 7600.
[14] P. Kowalczyk, R. Lech, M. Warecka, and A. Kusiek, "Electromagnetic plane wave scattering from a cylindrical object with an arbitrary cross section using a hybrid technique," *J. Electromagn. Waves Appl.*, pp. 1–15, 2018.

[15] M. Polewski, R. Lech, and J. Mazur, "Rigorous modal analysis of structures containing inhomogeneous dielectric cylinders," *IEEE Trans. Microw. Theory Techn.*, vol. 52, no. 5, pp. 1508–1516, May 2004.
[16] Y. Su, J. Wang, X. Zeng, Z. Bai, C. Chiang, and D. Zhou, "SAPOR: second-order Arnoldi method for passive order reduction of RCS circuits," in *Proc. Int. Conf. Comput.-Aided Design (ICCAD)*. IEEE Computer Society, Nov. 2004, pp. 74–79.
[17] B. N. Sheehan, "ENOR: Model order reduction of RLC circuits using nodal equations for efficient factorization," in *Proc. IEEE 36th Design Autom. Conf.* ACM, Jun. 1999, pp. 17–21.
[18] V. de la Rubia, "Reliable reduced-order model for fast frequency sweep in microwave circuits," *Electromagnetics*, vol. 34, no. 3-4, pp. 161–170, Apr. 2014.
[19] M. Hess and P. Benner, "Fast evaluation of time harmonic Maxwell's equations using the reduced basis method," *IEEE Trans. Microw. Theory Techn.*, vol. 61, no. 6, pp. 2265–2274, Jun. 2013.
[20] G. Fotyga, M. Czarniewska, A. Lamecki, and M. Mrozowski, "Reliable greedy multipoint model-order reduction techniques for finite-element analysis," *IEEE Antennas Wireless Propag. Lett.*, vol. 17, no. 5, pp. 821–824, May 2018.
[21] D. Szypulski, G. Fotyga, and M. Mrozowski, "An enhanced reduced basis method for wideband finite element method simulations," *IEEE Access*, vol. 7, pp. 60 877–60 884, May 2019.
[22] T. A. Davis, "Algorithm 832: UMFPACK V4.3—an unsymmetric-pattern multifrontal method," *ACM Trans. Math. Software*, vol. 30, no. 2, pp. 196–199, Jun. 2004.
[23] O. Schenk and K. Gärtner, "Solving unsymmetric sparse systems of linear equations with PARDISO," *Future Gener. Comput. Syst.*, vol. 20, no. 3, pp. 475–487, Apr. 2004.
[24] D. B. Davidson, *Computational Electromagnetics for RF and Microwave Engineering*. Cambridge university press, 2005.
[25] D. Deschrijver, M. Mrozowski, T. Dhaene, and D. De Zutter, "Macromodeling of multiport systems using a fast implementation of the vector fitting method," *IEEE Microw. Wireless Compon. Lett.*, vol. 18, no. 6, pp. 383–385, Jun. 2008.

Post-print of: Fotyga G., Szypulski D., Lechociński R., Kowalczyk P.: Communication Model Order Reduction in Hybrid Methods Involving Generalized Impedance Matrix IEEE TRANSACTIONS ON ANTENNAS AND PROPAGATION (2020), pp.1-7 DOI: 10.1109/TAP.2020.2970027